https://doi.org/10.1016/j.measurement.2020.108957

A Baseline-Free Damage Detection Method Using VBI Incomplete Measurement Data

Mohsen Mousavi[a,b], Damien Holloway *[a], J.C. Olivier[a], Amir H. Gandomi *[b]

[a] *School of Engineering, University of Tasmania, Hobart 7005, Tasmania, Australia*
[b] *Faculty of Engineering and IT, University of Technology Sydney, Ultimo, NSW 2007, Australia*

Abstract

A novel baseline-free method for damage detection of vehicle-bridge interaction (VBI) systems is proposed. The proposed method is physics-based, in contrast to many prevailing approaches, which are purely data-based techniques. It uses incomplete measurement data by incorporating the static condensation transformation matrix into the equations to obtain the final formulas. However, the static condensation of the damaged beam is not known *a priori*. Therefore, it is shown analytically that the static condensation transformation matrix of the undamaged beam can be used instead of the one corresponding to the damaged beam. This has been confirmed through numerical simulations for different boundary conditions of the beam. Various factors are studied numerically in order to demonstrate the robustness of the proposed method, including road roughness, boundary conditions, variable moving mass velocity and measurement noise. The results demonstrate the capability of the proposed method in damage detection of beam-type structures subjected to a moving mass in the presence of 5% noise. It has also been shown that averaging the results obtained from noisy data collected through several repetitions of the experiment can improve the final prediction of the location and severity of damage.

Keywords: `Vehicle-Bridge Interaction, Vibration, Damage Detection, Static Condensation, Incomplete Measurement`

Nomenclature

$[C]$ Beam global Damping matrix

$[I]$ Identity matrix

$[K]$ Beam global stiffness matrix

$[k_i]$ i^{th} beam local stiffness matrix

Email addresses: `Corresponding authors: damien.holloway@utas.edu.au` (Damien Holloway *), `gandomi@uts.edu.au` (Amir H. Gandomi *)

$[M]$	Beam global mass matrix
$[T]$	Static condensation transformation matrix of healthy structure
$[T_d]$	Static condensation transformation matrix of damaged structure
α_i	Stiffness reduction factor of the i^{th} element
β_i	$= 1 - \alpha_i$
ξ_b	Beam damping ratio
ξ_v	Damping ratio of the suspension system of the moving mass
ζ	Normalised location on an element
$\{\bar{F}\}$	Reduced static equivalent force vector
$\{\bar{U}\}$	Reduced static equivalent displacement vector
$\{f(t)\}$	Dynamic force vector
$\{F\}$	Static equivalent force vector
$\{N_c\}$	Contact point beam element shape vector
$\{u(t)\}$	Dynamic displacement vector
$\{U\}$	Static equivalent displacement vector
k_v	Stiffness of the moving mass suspension system
L_e	Length of each element
m_v	Vehicle mass
P	Applied force magnitude$= m_v \times g$
r_c	Contact point road roughness
V	Moving mass velocity

1. Introduction

Structural health monitoring (SHM) of beam structures is of great importance as they are typical models for structures such as bridges [1]. Several methods have been developed by researchers to address the SHM of such structures, which usually exploit information obtained from the beam vibration in the frequency-domain or time-domain. As an example of frequency domain data used for beam damage detection, structural mode shapes have been widely used [2, 3]. For instance, Janeliukstis et al. proposed a technique that uses continuous wavelet transform to study beam modal curvature for damage detection on beam type structures [4]. Likewise, time domain data have also been used for damage detection [5, 6]. Jiang et al. proposed a nonlinearity measure-based localisation technique based on a proper orthogonal decomposition technique for damage localisation on beam type structures [7]. There are, however, many such techniques that can only detect the location of the damage. Therefore, developing a technique to quantify the severity of the damage as well as its location is still a developing area in the realm of SHM of beam type structures [8].

Desirable SHM techniques rely on minimal or incomplete information about the structure. Hence, recent trends in SHM have been towards identifying a minimum set of data to be obtained from structures, and deriving useful information from them [9, 10, 11, 12]. However, this will require either new sensing technologies or novel computational and data analysis techniques [13, 14].

Computational sciences provide a wide range of new techniques that can be used to derive information from a few measured data points on structures. Many such techniques have been introduced in SHM, as reported by different researchers in the literature, some of which are (1) data analysis techniques such as Symbolic Dynamic Analysis (SDA) [15, 16, 17, 18, 19, 20], or (2) signal processing algorithms such as Wavelet Transform (WT) [21, 22], Empirical Mode Decomposition (EMD) [23, 24, 25] or variational mode decomposition (VMD) [26, 27]. Most of these techniques are used only to detect the location of damage.

SHM of bridge structures using a moving load has received a great deal of attention during the past decade. The main reason for this is that the required experiment to excite the structure is almost the same as its operational condition, making the whole procedure easy to carry out [28]. It also requires fewer sensors to be used [29]. Moreover, since the loading condition in such an experiment is deterministic, the experimental conditions are under control.

In such moving load experiments, the dynamic vibration of a beam can generally be divided into two stages: the time interval when the load is moving over the beam, and the subsequent free vibration of the beam after the load has completely passed over it.

Most damage detection procedures use vibration data recorded during the first stage [30, 31]. It is also known that higher frequency components of a structure's response are more sensitive to the damage [25]. Exploiting this fact, researchers have studied high frequency components for any changes that can be referred to damage on the beam. These components may be derived by decomposition techniques such as wavelet (WT) [21] or Hilbert-Huang transforms (HHT) [32] of the dynamic deflections of the beam. As such, damage can generally be detected as a peak at the time when the load moves over a cracked section [33, 34]. Unfortunately, more often than not, these peaks are very insignificant when considering noisy measurements or road roughness effects. To address this issue, baseline data obtained from the same experiment conducted on the undamaged beam is used by some researchers [30, 8, 35, 30]. However, it has been reported in the literature that any discrepancies between the velocity of the moving mass in the experiment conducted on the damaged and undamaged beam can interfere with the damage detection [36, 37].

On the other hand, the second stage of the free vibration of the beam after a moving load has traversed it seems to be overlooked in the literature. As an alternative to considering these two stages separately, therefore, the equivalent static formulation of the dynamic vibration of beam structures can be used for damage detection [38, 39]. As such, a continuous monitoring of the structure at both stages of the forced and subsequent free vibration of the structure is used in this paper.

This static equivalent equation requires less information about the structure when used for damage detection or parameter identification purposes. It is demonstrated in this paper that this strategy is a valid way of monitoring a beam type structure for damage when subjected to a moving mass.

To use the proposed method, the information required for conducting damage detection is limited only to the stiffness matrix; no information about the mass and damping matrices are required. Reducing the required information from the FE model of the intact structure has also been addressed by other researchers [40]. Some other researchers propose completely a non-model-based damage detection strategy [41]. The other advantage of the proposed technique of this paper is that it is baseline-free.

There are generally two models for the VBI problem, namely moving load or moving mass models. Accordingly, the term moving load refers to the case when the inertia forces of the load (and therefore, its interaction with the bridge) are neglected, while a moving mass model takes this inertia effect into account [42]. Yang and Lin mention that the vehicle mass can be neglected compared to the mass of the bridge [43]. It is shown in this paper that this is also true for the proposed method as while the proposed method was developed using a moving load model, it has subsequently been fully tested using a moving mass simulation in order to account for road roughness.

The main objective of the present paper, therefore, can be summarised as to propose a baseline-free damage detection strategy that can determine both damage location and severity with minimum information about the beam mechanical properties and experimental data. One of the advantage of using numerical methods in studying damage detection is that Monte Carlo simulations can easily be applied for better evaluation of these methods [44]. As such, a VBI model is studied and the effect of road roughness and the moving mass inertia are taken into account in all simulations.

The organisation of this paper is as follows:

In Section 2, the proposed damage detection method is explained, which consists of (1) equivalent static formulation of the dynamic vibration (Subsection 2.1), (2) a brief review of different methods for simulating damage in structures and choice of a general damage model (Subsection 2.2), (3) a formula for calculation of the damage indices (Subsection 2.3), followed by (4) some analytical investigation of the proposed formula (Subsection 2.4), and (5) proposal of an easy way to obtain the equivalent static force vector corresponding to the moving load with a steady velocity, in which a formula is derived to calculate the equivalent force for beams with different boundary conditions (Subsection 2.5). In Section 3, a VBI model considering road roughness and the interaction between the moving mass and beam is presented, which is used for evaluation of the proposed method. Section 4 is dedicated to (1) the numerical study of the undamaged and damaged cases with different beam boundary conditions, including and excluding the road roughness effect (Subsection 4.1), (2) a Monte Carlo study of the effect of noisy measurements on damage detection results (Subsection 4.2), and (3) the effect of substantial variations in the velocity of the moving mass used for damage detection (Subsection 4.4). In Section 5 some conclusions and possible future work are discussed.

2. The proposed damage detection technique

2.1. Equivalent static form of the governing equation

In this section, the equivalent static formulation of the dynamic vibration of a beam subjected to a moving load is discussed, to be used subsequently for damage detection on the beam. The derivation is summarised below. The differential equation of the vibration of the beam is well known and may be written as

$$[M]\{\ddot{u}(t)\} + [C]\{\dot{u}(t)\} + [K]\{u(t)\} = \{f(t)\}\,, \tag{1}$$

Following the first authors' previous work [39], to eliminate time dependence, hence obtain a static form of the equation, the spatially discretised dynamic equation of motion for the continuous beam in FE form can be integrated (Equation 1) with respect to time over the interval $0 \leq t \leq \infty$, where for practical purposes infinity may refer to the time when the beam has effectively stopped vibrating, some time after the load reaches the other end of the beam. Hence, Equation 1 becomes

$$[M]\left(\{\dot{u}(\infty)\} - \{\dot{u}(0)\}\right) + [C]\left(\{u(\infty)\} - \{u(0)\}\right) + [K]\{U\} = \{F\}\,, \tag{2}$$

where

$$\begin{aligned} \{U\} &= \int_0^\infty \{u(t)\}\,dt\,, \\ \{F\} &= \int_0^\infty \{f(t)\}\,dt\,. \end{aligned} \tag{3}$$

By applying the initial and final conditions of no displacement or velocity anywhere on the beam, i.e. $\{\dot{u}(0)\} = \{\dot{u}(\infty)\} = \{u(0)\} = \{u(\infty)\} = \{0\}$, this reduces to

$$[K]\{U\} = \{F\}\,. \tag{4}$$

Equation 4, is called the equivalent static formulation of the dynamic vibration of an FE model.

2.2. Simulation of damage in an element

Damage in this context is any modification to the structure that produces a local reduction of stiffness. It could for example include fatigue cracks, local buckling damage, severe local corrosion, or structural modifications. Any such localised defect can be modelled as an equivalent local reduction of the effective flexural rigidity EI [45].

In the FE analysis of the global response of damaged beams, it is sufficient to model localised damage as a uniform reduction of the stiffness of a single whole element. Accordingly, the flexural rigidity EI of the affected element, or equivalently the whole element stiffness matrix $[k_i]$, is factored.

In this paper, a stiffness reduction factor α is used, which takes values between 0 and 1, representing respectively an undamaged element and full loss of the stiffness of the element. Accordingly, the stiffness matrix of each element in global coordinates, $[k_i]$, is multiplied by its corresponding stiffness reduction factor, α_i, to obtain the global stiffness matrix for the damaged structure, $[K_d]$, as

$$[K_d] = [K] - \sum_{i=1}^{n_e} \alpha_i [k_i]\,. \tag{5}$$

Alternatively, the above equation can be simplified by introducing $\beta_i = 1 - \alpha_i$, hence

$$[K_d] = \sum_{i=1}^{n_e} \beta_i [k_i]\,. \tag{6}$$

2.3. Solving for the damage indices

By replacing the stiffness matrix of the pristine structure $[K]$ in Equation 4 with the stiffness matrix of the damaged structure $[K_d]$, as defined in Equation 6, and some algebraic simplification one can obtain [39],

$$\{\beta\}_{n_e \times 1} = [[k_1]\{U\} \ \ldots \ [k_{n_e}]\{U\}]^{+}_{n_e \times n_d} \times \{F\}_{n_d \times 1}\,, \tag{7}$$

where

$$\{\beta\} = \{\beta_1 \ \beta_2 \ \ldots \ \beta_{n_e}\}^{\tau}_{n_e \times 1}\,,$$

and in which $+$ is the Moore-Penrose pseudoinverse, a generalisation of the concept of an inverse for a non-square matrix [46], such as above. Also, τ represents the transpose of a matrix or a vector.

In order to obtain the damage indices in Equation 7, information about all DOFs of the structure is required. However, generally it is difficult to measure rotational DOFs. In this case we choose the translational DOFs to be the master DOFs, and the rotations to be the slave DOFs. The transformation matrix of the static condensation scheme $[T]$ obtained from the global stiffness matrix of the structure can be used to remove slave DOFs

$$[T]_{n_d \times m} = \begin{bmatrix} [I]_{m \times m} \\ -[K]^{-1}_{s \times s}[K]_{s \times m} \end{bmatrix}. \tag{8}$$

Here, m and s are the numbers of master and slave DOFs, $[K]_{s \times s}$ is the stiffness matrix with rows and columns corresponding to master DOFs removed (slave DOFs retained), while $[K]_{s \times m}$ had master rows and slave columns removed. However, since the beam is damaged, the static transformation matrix $[T_d]$ must be used. Using this transformation one can then write

$$\{\beta\}_{n_e \times 1} = [\Lambda]^{+}_{n_e \times m}\{\overline{F}\}_{m \times 1}\,, \tag{9}$$

where

$$[\Lambda] = [[T_d]^{\tau}[k_1][T_d]\{\overline{U}\} \ \ldots \ [T_d]^{\tau}[k_{n_e}][T_d]\{\overline{U}\}]_{m \times n_e} \tag{10}$$

and $\{\overline{U}\}$ is the integrated displacement vector at only the master DOFs. Note that each of the components $[T_d]^{\tau}[k_i][T_d]\{\overline{U}\}$, $i = 1, 2, \ldots, n_e$, is an $m \times 1$ column vector, hence $[\Lambda]$ is $m \times n_e$. Also, in Equation 9, $\{\overline{F}\}$ is the static condensation force vector obtained from the following formula,

$$\{\overline{F}\} = \{F_m\} - [K_d]_{m \times s}[K_d]^{-1}_{s \times s}\{F_s\}\,. \tag{11}$$

Note that in the above equation, $\{F_m\}$ and $\{F_s\}$ are the force vectors applied to the master and slave DOFs, respectively.

As can be seen from Equation 8, the transformation matrix of the static condensation scheme depends only on the system stiffness matrix. However, since $[T_d]$ is obtained based on $[K_d]$, it is also a function of $\{\beta\}$.

Notwithstanding this, it is next demonstrated that using $[T]$ instead of $[T_d]$ provides a good approximation. Similarly, it may also be concluded that constructing $[K]_{m\times s}[K]^{-1}_{s\times s}$ using $[K]$ produces a good approximation.

2.4. A rationale for using $[T]$ instead of $[T_d]$

It can be seen from Equation 10 that matrix $[\Lambda]^{+}_{n_e\times n_d}$ is a function of $\{\beta\}$ as it includes the transformation matrix $[T_d]$. Hence, in this section we aim at showing that using $[T]$ instead of $[T_d]$ is a good approximation. As such, the transformation matrix of the static condensation of a damaged structure $[T_d]$ from Equation 8 can be written in the form

$$[T_d]_{n_d\times m} = \begin{bmatrix} [I]_{m\times m} \\ \sum_{i=1}^{n_e} -(\beta_i[k_i]_{s\times s})^{-1} \times \sum_{i=1}^{n_e} \beta_i[k_i]_{s\times m} \end{bmatrix}, \tag{12}$$

or equivalently,

$$[T_d]_{n_d\times m} = \begin{bmatrix} [I]_{m\times m} \\ -([A]\ [B])^{-1} \times ([A]\ [C]) \end{bmatrix} \tag{13}$$

in which

$$[A] = \begin{bmatrix} [\beta_1]_{s\times s} & [\beta_2]_{s\times s} & \cdots & [\beta_{n_e}]_{s\times s} \end{bmatrix}_{s\times(n_e\times s)} \tag{14}$$

$$[B] = \begin{bmatrix} [k_1]_{s\times s} & [k_2]_{s\times s} & \cdots & [k_{n_e}]_{s\times s} \end{bmatrix}^{\tau}_{(n_e\times s)\times s} \tag{15}$$

$$[C] = \begin{bmatrix} [k_1]_{s\times m} & [k_2]_{s\times m} & \cdots & [k_{n_e}]_{s\times m} \end{bmatrix}^{\tau}_{(n_e\times s)\times m} \tag{16}$$

and $[\alpha_i]_{ss} = \alpha_i I_{ss}$.

In Equation 13, $[A]$ and $[B]$ are not square matrices. However $[A]$ and $[B]$ are full row and column ranked matrices, and thus have right and left Moore-Penrose inverses respectively, namely $[A]^+ = [A]^\tau([A][A]^\tau)^{-1}$ and $[B]^+ = ([B][B]^\tau)^{-1}[B]^\tau$. Because $[A]$ has linearly independent rows, but not columns, it does not have a left inverse. However, although $[A]^+[A]$ is not equal to the general identity matrix $[I]_{(ne\times s)(ne\times s)}$, it *is* the closest that one can achieve [47]. We can therefore approximate $([A][B])^{-1} \approx [B]^+[A]^+$, and write

$$[T]_{n_d\times m} \approx \begin{bmatrix} [I]_{m\times m} \\ -[B]^+\,[A]^+\,[A]\,[C] \end{bmatrix} \approx \begin{bmatrix} [I]_{m\times m} \\ -[B]^+\,[C] \end{bmatrix}. \tag{17}$$

Since damage affects only matrix $[A]$, which is not present in Equation 17, this shows that using $[T]$ instead of $[T_d]$ brings about a good approximation.

Similarly, it can be shown that constructing $[K]_{m\times s}[K]^{-1}_{s\times s}$ using the stiffness matrix of the intact beam $[K]$ is a good assumption.

Therefore $[\Lambda]$ and $\{\overline{F}\}$ in Equations 10 and 11 can be obtained respectively as

$$[\Lambda] = [[T]^{\tau}[k_1][T]\{\overline{U}\} \; \dots \; [T]^{\tau}[k_{n_e}][T]\{\overline{U}\}]_{m\times n_e} \tag{18}$$

and

$$\{\overline{F}\} = \{F_m\} - [K]_{m\times s}[K]^{-1}_{s\times s}\{F_s\}\,. \tag{19}$$

Finally the unknown damage indices $\{\beta\}$ can be found by substituting Equations 18 and 19 into the Equation 9. However, the derivation of $\{F_m\}$ and $\{F_s\}$ in Equation 19 is still unknown. The procedure of obtaining these vectors is discussed in the following section.

2.5. Calculation of the equivalent static force vector

The beam can be discretised into a number n_e of beam elements, each with four degrees of freedom, as shown in Figure 1. In order to construct the FE model, the deflection within an element can be written in terms of shape functions N_k as $u(x) = \sum_{k=1}^{4} u_j N_k(\zeta) = \{N\}^{\tau}\{u\}$, where $x = \zeta L_e$ $(0 \le \zeta \le 1)$ is the distance along the element from left to right, $k = 1 \dots 4$ are the indices of the elemental degrees of freedom, and $j = 2(i-1)+k$ are the corresponding global degrees of freedom for element i. Here $k = 1$ and $k = 3$ correspond to the element's left and right end vertical displacements, while $k = 2$ and $k = 4$ are the left and right end rotations. The Hermite cubic Shape functions are used [48], which are

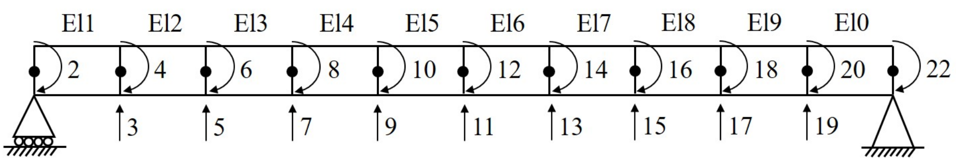

Figure 1: An example of a simply supported beam discretised into ten beam elements with translational and rotational DOFs at each node. Note that DOFs 1 and 21 are restrained in this example, hence are not shown.

$$\begin{aligned} N_1 &= 1 - 3\zeta^2 + 2\zeta^3 \\ N_2 &= L_e\left(\zeta - 2\zeta^2 + \zeta^3\right) \\ N_3 &= 3\zeta^2 - 2\zeta^3 \\ N_4 &= L_e\left(-\zeta^2 + \zeta^3\right) \end{aligned} \tag{20}$$

where in above equations, L_e is the element length and ζ is the normalised element-wise local coordinate taking values between 0 and 1.

In order to find the force vector corresponding to the moving load on each translational DOF, the following procedure is followed:

Without loss of the generality it is assumed that the velocity of the moving mass is constant. Therefore, for a moving load P with constant velocity V, the time taken for the load to pass over the element is equal to L_e/V and the load's relative position is $\zeta = V(t - t_{i-1})/L_e$, where $t_{i-1} \leq t \leq t_i$, and t_{i-1} and t_i are the times at which the load passes the $(i-1)^{th}$ and i^{th} nodes, respectively, which define the i^{th} element. The applied load on the element can then be distributed to the DOFs of that element by multiplying the force P by the corresponding shape functions evaluated at the load's relative position ζ. The component of the load applied to all DOFs not associated with the loaded element is equal to zero. Hence, the force vector when the mass moves over the i^{th} element is

$$\{f(t)\} = \begin{Bmatrix} 0 \\ \vdots \\ 0 \\ PN_1^i(\zeta) \\ PN_2^i(\zeta) \\ PN_3^i(\zeta) \\ PN_4^i(\zeta) \\ 0 \\ \vdots \\ 0 \end{Bmatrix} \tag{21}$$

where the superscript i on function N_k indicates these are applied to the DOFs applicable to element i. Accordingly, the force vector should be updated as the load reaches the next element.

Equation 21 can be also presented in a more compacted form as,

$$f_j(t) = \begin{cases} 0 & \text{if } j \leq 2(i-1) \text{ or } j > 2(i+1) \\ PN_k^i(\zeta) & j = 2(i-1) + k\,, \quad k = 1 \ldots 4 \end{cases} \tag{22}$$

where $j = 1 \ldots n_d$ $(n_d = 2(n_e + 1))$ represents the DOF; $i = 1 \ldots n_e$ represents the element on which the load currently acts (i.e. $t_i \leq t \leq t_{i+1}$); $k = 1 \ldots 4$ represent respectively the left deflection, left rotation, right deflection and right rotation of the end nodes of element i; and L_e in Equation 20 is taken to be the length of element i, which in this implementation is assumed to be the same for all elements.

Substituting Equation 21 into Equation 3 gives us the equivalent static force acting on the beam due to the moving load in terms of the shape functions N_k defined in Equation 20. It is apparent from Equation 21 that $f_j(t)$ is nonzero only during the time that the moving load is on one of the two elements that share the node corresponding to DOF j. Hence for the general case, using Equation 4 and before imposing boundary conditions one may obtain F as

$$\{F\} = \left\{ \begin{array}{c} \int_{t_0}^{t_1} PN_1^1 \, dt \\ \int_{t_0}^{t_1} PN_2^1 \, dt \\ \int_{t_0}^{t_1} PN_3^1 \, dt + \int_{t_1}^{t_2} PN_1^2 \, dt \\ \int_{t_0}^{t_1} PN_4^1 \, dt + \int_{t_1}^{t_2} PN_2^2 \, dt \\ \vdots \\ \int_{t_{i-2}}^{t_{i-1}} PN_3^{i-1} \, dt + \int_{t_{i-1}}^{t_i} PN_1^i \, dt \\ \int_{t_{i-2}}^{t_{i-1}} PN_4^{i-1} \, dt + \int_{t_{i-1}}^{t_i} PN_2^i \, dt \\ \vdots \\ \int_{t_{ne-1}}^{t_{ne}} PN_3^{ne} \, dt \\ \int_{t_{ne-1}}^{t_{ne}} PN_4^{ne} \, dt \end{array} \right\}. \tag{23}$$

In Equation 23, as stated above, $t_0 = 0$, t_i is the time when the load arrives at the first node of the $(i+1)^{th}$ element, and t_{n_e} is the time when the load reaches the far end of the beam. For a simply supported beam, the first and penultimate degrees of freedom are deleted.

If the velocity V of the moving force is constant and the beam is divided into equal-length elements, then we note that on element i, $t = t_{i-1} + \frac{L_e}{V}\zeta$, hence $\int_{t_{i-1}}^{t_i} PN_k^i \, dt = \frac{PL_e}{V} \int_0^1 N_k \, d\zeta$. For $k = 1, 2, 3, 4$ respectively, this evaluates to $\frac{PL_e}{2V}, \frac{PL_e^2}{12V}, \frac{PL_e}{2V}, \frac{-PL_e^2}{12V}$, so we can write

$$\begin{aligned} \int_{t_{i-2}}^{t_{i-1}} PN_3^{i-1} \, dt + \int_{t_{i-1}}^{t_i} PN_1^i \, dt &= \frac{PL_e}{V} \\ \text{and} \quad \int_{t_{i-2}}^{t_{i-1}} PN_4^{i-1} \, dt + \int_{t_{i-1}}^{t_i} PN_2^i \, dt &= 0 \, . \end{aligned} \tag{24}$$

Finally, noting that the translational DOFs are the master and the rotational DOFs are the slave DOFs, the reduced force vector $\overline{F}$ is obtained as,

$$\{\overline{F}\} = \left\{ \begin{array}{c} \frac{PL_e}{V} \\ \vdots \\ \gamma \, \frac{PL_e}{V} \end{array} \right\}_{m\times 1} - [K_{ms}][K_{ss}]^{-1} \left\{ \begin{array}{c} \eta \, \frac{PL_e^2}{12V} \\ 0 \\ \vdots \\ \lambda \, \frac{-PL_e^2}{12V} \end{array} \right\}_{s\times 1} \tag{25}$$

where γ, η, and λ are constants characterising the beam boundary conditions. For each studied combination of boundary conditions (see Figure 2) with a constant moving mass velocity these are:

1. Simple-Simple (SS): $\gamma = 1$, $\eta = 1$, and $\lambda = 1$;
2. Clamped-Simple (CS): $\gamma = 1$, $\eta = 0$, and $\lambda = 1$;
3. Clamped-Clamped (CC): $\gamma = 1$, $\eta = 0$, and $\lambda = 0$;

4. Clamped-Free (CF): $\gamma = \frac{1}{2}$, $\eta = 0$, and $\lambda = 1$ (included here for completeness, though it would not exist for a bridge in practice).

Note that the numbers of master (m) and slave (s) DOFs vary from one boundary condition to another.

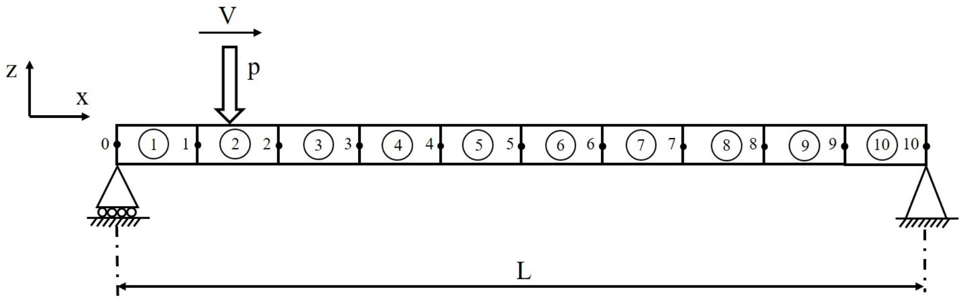

(a) Simple-Simple

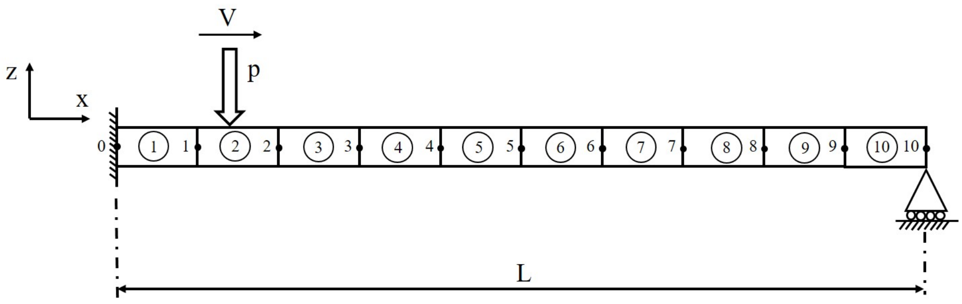

(b) Clamped-Simple

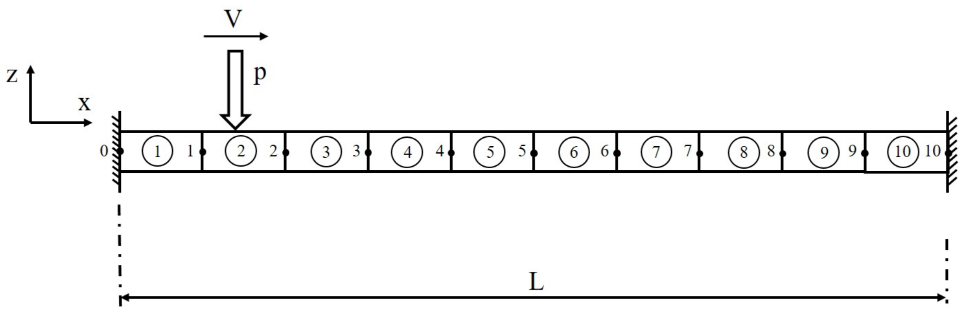

(c) Clamped-Clamped

Figure 2: Different boundary conditions of the studied beam.

Finally, the procedure of the proposed method can be summarised as follows,

1. Measure displacement time history of the beam $u(t)$ subjected to a moving mass at some points on the beam for the time duration when the experiment begins to when the vibration of the beam is fully damped out.
2. Use Equation 3 to compute the static equivalent deflection of the beam $\{\overline{U}\}$ for each measured point at only translational DOFs.

https://doi.org/10.1016/j.measurement.2020.108957

3. Use Equation 25 to obtain the condensed static equivalent force vector $\{\overline{F}\}$ applied to the measured DOFs.
4. Compute the vector $[\Lambda]$ from the Equation 18.
5. Finally, use Equation 9 to compute unknown damage indices $\{\beta\}$ by inserting $[\Lambda]$ and $\{\overline{F}\}$ obtained from the previous stages.

2.6. Overview of the proposed method

In this section, an overview of the proposed method is provided for the convenience of the reader, and is illustrated in Figure 3.

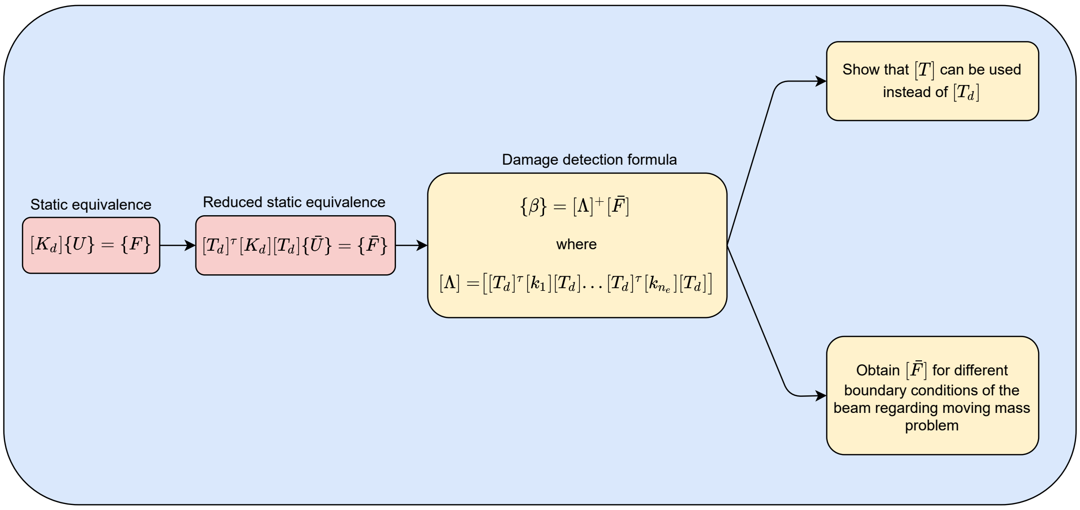

Figure 3: An overview of the scheme of the paper.

As depicted in the figure, the first step is to obtain the static equivalent formulation of the beam vibration, as discussed in Section 2.1. Next, a reduced form of the equations is obtained using the static condensation transformation matrix (see Section 2.3). These first two steps (in darker color) were developed and discussed in the authors' previous work [39]. However, in the previous work, an iterative method was proposed for damage detection as the static condensation transformation matrix $[T_d]$, itself is a function of the damage indices (matrix $[\beta]$). In order to propose a direct formula for damage detection, we demonstrated in Section 2.4 that the static condensation transformation matrix of the intact beam $[T]$ can be used instead of the one corresponding to the defective beam, i.e. $[T_d]$. Finally, the equation for $[\bar{F}]$ for the moving mass experiment is required, which is derived and discussed in Section 2.5 for various boundary conditions.

In the next section, we use numerical simulation to demonstrate the capability of the proposed method in damage detection of a beam with different boundary conditions using a driveby sprung mass. The so called VBI model includes the effect of the road roughness as well as the moving mass inertia, and is used later for all simulations to examine the capability of the proposed method.

3. Vehicle Bridge Interaction (VBI) simulation considering road roughness

Figure 4 shows a FE model of the VBI model which is used for evaluation of the proposed method (see [31]). According to the model, a sprung mass m_v with the stiffness k_v and damping

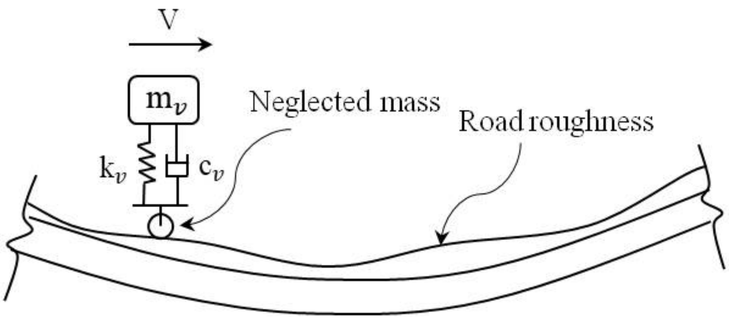

Figure 4: Moving mass with suspension system over a bridge with rough surface.

ratio ξ_v is supposed to traverse the beam at constant velocity. To simulate the beam vibration, Hermite cubic shape functions of Equation 20 are used.

The cubic Hermitian interpolation vector $\{N_c\}$ is then evaluated at the contact point and used in the following FE model,

$$\begin{bmatrix} m_v & 0 \\ 0 & [M] \end{bmatrix} \begin{Bmatrix} \ddot{y}_v \\ \{\ddot{u}\} \end{Bmatrix} + \begin{bmatrix} c_v & -c_v\{N_c\}^\tau \\ -c_v\{N_c\} & [C]+c_v\{N_c\}\{N_c\}^\tau \end{bmatrix} \begin{Bmatrix} \dot{y}_v \\ \{\dot{u}\} \end{Bmatrix}$$
$$+ \begin{bmatrix} k_v & -c_vV\{N_c'\}^\tau - k_v\{N_c\}^\tau \\ -k_v\{N_c\} & [K]+c_vV\{N_c\}\{N_c'\}^\tau + k_v\{N_c\}\{N_c\}^\tau \end{bmatrix} \begin{Bmatrix} y_v \\ \{u\} \end{Bmatrix} \tag{26}$$
$$= \begin{Bmatrix} c_vVr_c' + k_vr_c \\ -c_vVr_c'\{N_c\} - k_vr_c\{N_c\} - m_vg\{N_c\} \end{Bmatrix}$$

where, reiterated, $[M]$, $[C]$, and $[K]$ are the mass, damping and stiffness matrices of the beam FE model, respectively. The superscript $'$ represents the derivative of a matrix with respect to its location on the beam. The terms y_v and $\{u\}$ correspond respectively to the vertical displacements of the moving mass and the nodal degrees of freedom of the beam elements. c_v is the suspension system damping coefficient which is obtained from $2m_v\xi_v\sqrt{k_v/m_v}$ (See Table 1). A Rayleigh damping model, i.e. of the form $[C] = a[M] + b[K]$ is considered for the beam. Note though that the vehicle suspension characteristics and bridge mass and damping matrices are used only for the simulation, and are not required for the proposed damage detection procedure. Finally, r_c is an artificial road roughness generated by the following equation based on ISO 8608 [49],

$$r_c(x) = \sum_{i=0}^{N} 2^k \times 10^{-3} \times \sqrt{\Delta n} \left(\frac{n_0}{i\Delta n}\right) \cos\left(2\pi i \Delta n x + \phi_i\right), \tag{27}$$

where the constant $(2^k \times 10^{-3})$ has units $\mathrm{m}^{3/2}$ and Δn has units m^{-1}, hence r_c has units m. The constant scalar k is the ISO road profile quality measure and can take an integers from 3 to 9 reflecting the profiles from class cl_1 to class cl_8. Note that in this paper, a road profile of class cl_1 is considered for simulations, i.e. $k = 3$). Moreover, it is assumed $n_0 = 0.1\ \mathrm{m}^{-1}$. Abscissa x denotes the location on the road with respect to the reference point. The random phase angle ϕ_i has a uniform probabilistic distribution and takes a value within the range of 0 to 2π. Also $N = L/B$ and $\Delta n = 1/L$ in which L and B are the length of the road profile and the wavelength of the shortest spatial component of the roughness profile, respectively. This form of road roughness has been considered by other researchers [31].

A Matlab program has been developed based on the Newmark constant average acceleration method in order to numerically simulate the vibration time history of beams with different boundary conditions. Then, the deflection of the beam at translational DOFs are used to calculate the static equivalent response of the beam using Equation 4.

4. Numerical results and discussions

In this section numerical simulations of a beam with the properties presented in Table 1 are used for damage detection using the VBI model presented in Section 3. It is assumed that 10 sensors are available. Therefore, the beam is divided into 10 beam elements with rotational and translational degrees of freedom at each node (see Figure 1). It is obvious that the beam can be divided into fewer or more elements based on the number of available sensors. Also in the case of having a limited number of sensors, one can repeat the experiment to refine the possible region of damage.

In order to achieve a reasonable initial condition at the start of traverse of the mass across the beam, it is assumed that the mass has been moving over the rough road with a length equal to the length of the beam L before it arrives at the left hand side of the beam, and continues moving over the beam until it reaches the other side. Therefore, a road profile for a length of $2L$ is generated and used in simulations as presented in Figure 5.

The effects on results of the following aspects are investigated:

1. boundary conditions;
2. noisy measurements;

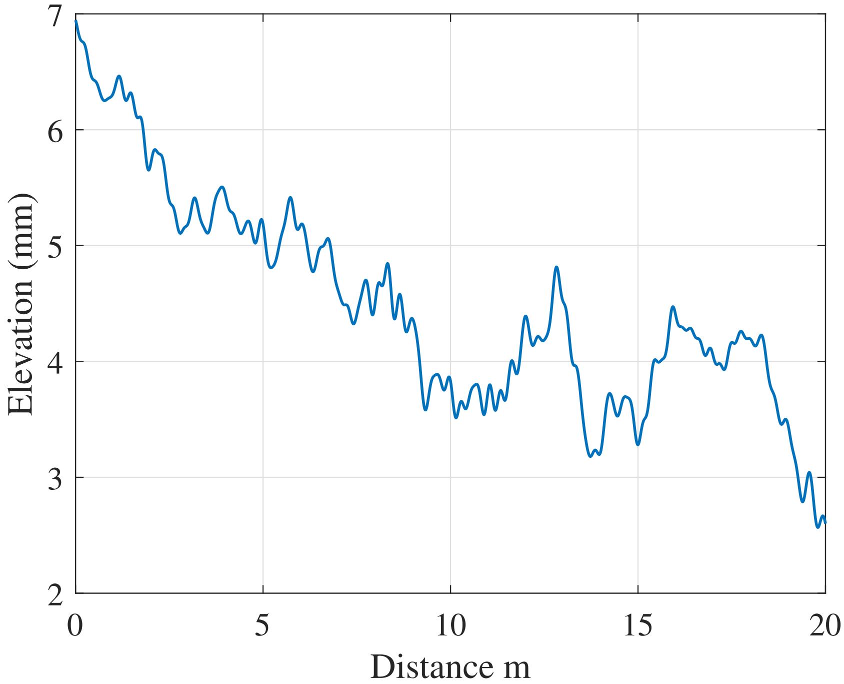

Figure 5: Road roughness profile used in simulations, starting one beam length ($L = 10$ m) before the left end of the beam and ending at the right end of the beam. The beam spans from 10 m to 20 m.

3. variable moving mass velocity.

In the first two cases the velocity of the moving load was fixed at 2 m/s. Therefore, it takes 5 seconds for the load to cross the beam. The beam is monitored until the vibration decays to an acceptable rate close to zero for each simulation. Two cases are considered for each scenario: the undamaged and damaged beams. For the damaged case, in order to consider different simultaneous damage positions on the beam and different damage indices, it is assumed that damage is present in elements 5 and 9, with severity $\alpha_5 = 0.2$ and $\alpha_9 = 0.25$.

4.1. Effect of different boundary conditions on results

In order to investigate how boundary conditions can affect the results, three different scenarios are studied in this section: *Simple–Simple* (SS), *Clamped–Simple* (CS), and *Clamped–Clamped* (CC), shown in Figure 2.

Table 2 shows the three first natural frequencies of the undamaged beam with these different boundary conditions.

The Rayleigh damping constants a and b were set to achieve the target damping ratio as specified in Table 1 which is assumed to be equal to 5% at the first two natural frequencies of the beam. The Rayleigh damping coefficients are calculated for each boundary condition combination, and are shown in Table 3.

Quantity	**Symbol**	**Value**
Beam modulus of elasticity	E	200 GPa
Beam density	ρ	7800 kg/m^3
Beam damping ratio	ξ_b	5%
Beam length	L	10 m
Beam cross-section height	h	0.5 m
Beam cross-section width	w	0.5 m
Moving mass magnitude	m_v	200 kg
Moving mass velocity	V	2 m/s
Suspension stiffness	k_v	20 kN
Suspension damping	ξ_v	10%
Sampling frequency	S_f	1 KHz

Table 1: VBI simulation model constants.

	SS	CS	CC
1st	4.59	7.17	10.41
2nd	18.37	23.25	28.70
3rd	41.35	48.54	56.31

Table 2: Natural frequencies (Hz) for different boundary conditions of the undamaged beam.

Using the presented VBI model in Section 3, the vibration time history of the beam at all DOFs is simulated. The beam is monitored at least for 10 seconds in all cases until the vibration of the beam is fully damped.

The damage scenario mentioned earlier is considered and Figure 6 shows the simulated deflection time history of the intact and damaged beam with the different boundary conditions at its midspan (node 5), with and without road roughness included.

We now consider the values of the damage indices predicted for both undamaged and damaged scenarios—Figures 7 and 8 respectively show these for the different boundary conditions.

It is noted that α_i values for the undamaged scenario should ideally all be zero (Figure 7), while in the damaged scenario the ideal α_i values should also be zero except for α_5 and α_9. As mentioned above, the assumed damage is that elements 5 and 9 lose respectively 20% and 25% of their stiffness, shown in yellow in Figure 8 for comparison.

Perfect results are not expected due to the fact that using incomplete data will not result in an exact solution. In particular, the existence of negative damage indices is not physically

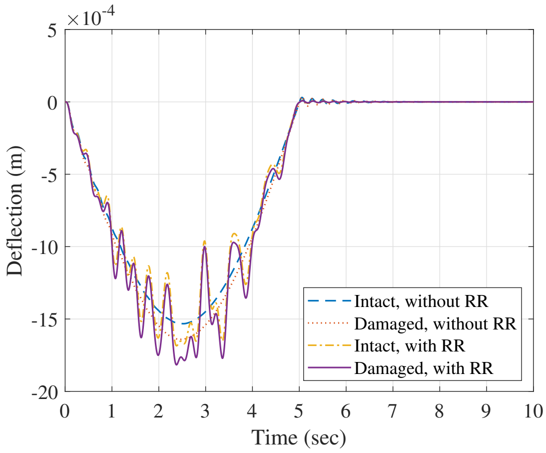

(a) Simple-Simple

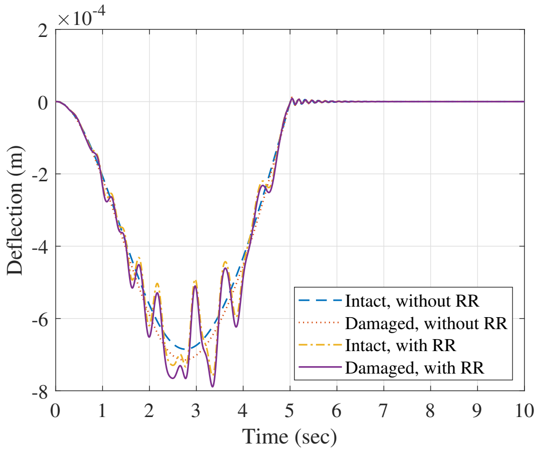

(b) Clamped-Simple

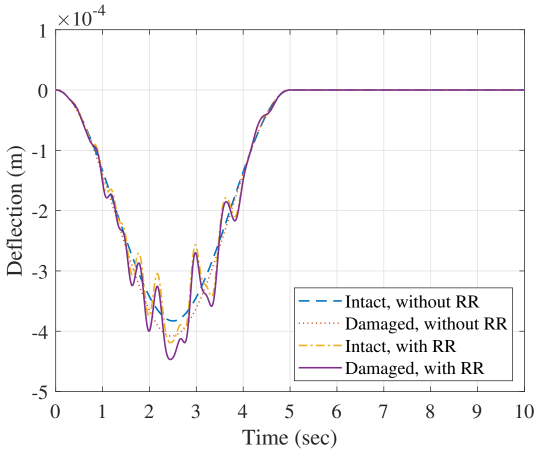

(c) Clamped-Clamped

Figure 6: Deflection time history at beam mid-span (node 5) subjected to a mass moving at 2 m/s, for different boundary conditions, with and without road roughness, for the intact and damaged beams, when elements 5 and 9 are damaged respectively with 20% and 25% loss of stiffness.

	SS	CS	CC
a	2.3084	3.4448	4.8001
b	0.0007	0.0005	0.0004

Table 3: Calculated Rayleigh damping coefficients for different boundary conditions of the undamaged beam.

meaningful. Therefore, it is suggested that these negative values are ignored and considered as zero damage, as suggested in [50]. Considering this we see excellent qualitative agreement.

While Figures 7 and 8 give a good qualitative overview, in order to compare the accuracy of each method quantitatively an accuracy index AI is used, based on the Euclidean norm of the difference between calculated and real damage indices. This can be written as

$$AI = 1 - \sqrt{\frac{1}{n_e}\sum_{i=1}^{n_e}(\alpha_i^s - \alpha_i^c)^2} \tag{28}$$

where α_i^s and α_i^c are respectively the simulated and calculated i^{th} damage index. A value of $AI = 1$ indicates a perfect prediction. Note that in Equation 28 the negative damage indices are also taken into account.

Boundary condition	**HS**	**HRR**	**DS**	**DRR**
SS	0.9796	0.9794	0.9768	0.9768
CS	0.9688	0.9682	0.9811	0.9809
CC	0.9796	0.9787	0.9773	0.9765

Table 4: Accuracy indices (AI) calculated for different boundary conditions for healthy smooth (HS), healthy with road roughness (HRR), damaged smooth (DS), and damaged with road roughness (DRR) beams.

The calculated values of AI corresponding to the 16 different scenarios are presented in Table 4. Accordingly, the following observations may be made:

1. In all cases the accuracy for the damaged scenarios is less than for the healthy scenarios except for the CS case, but only very slightly.
2. The accuracy corresponding to SS and CC in all cases are very similar. One reason might be due to the symmetry of the boundary conditions.
3. In all cases the accuracy of the results obtained for all scenarios without road roughness (RR) is at least equal (damaged SS) or better than the ones with road roughness. However, there is only ever a very small difference between the two cases, so it appears that road roughness has an almost negligible detrimental effect on results.

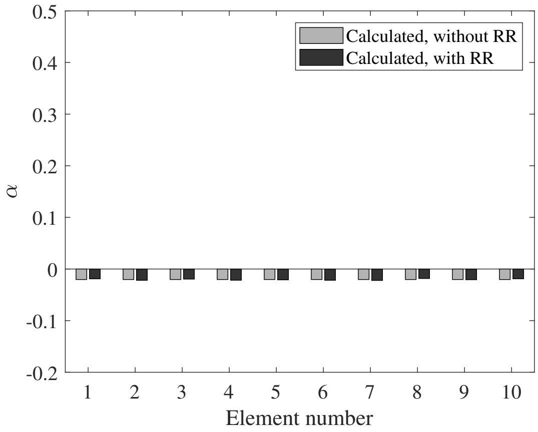

(a) Simple-Simple

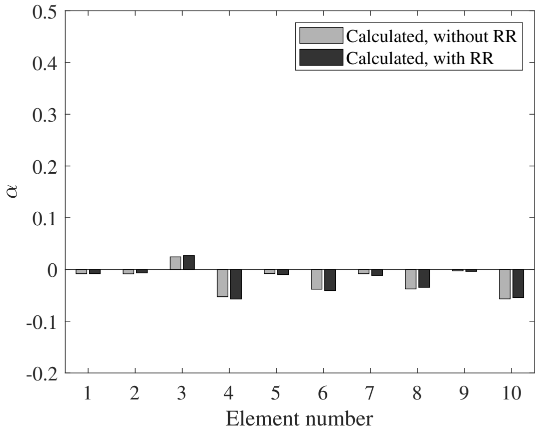

(b) Clamped-Simple

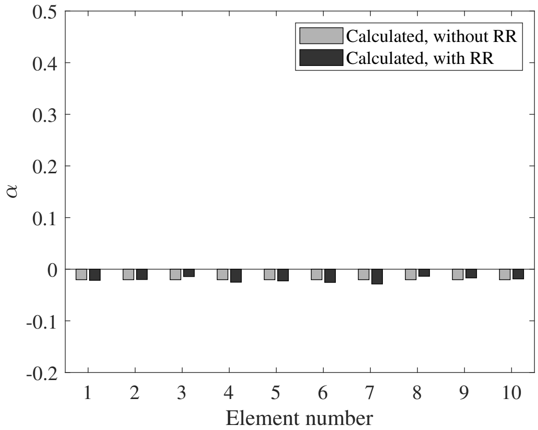

(c) Clamped-Clamped

Figure 7: Calculated damage for the undamaged scenario of the beam with different boundary conditions.

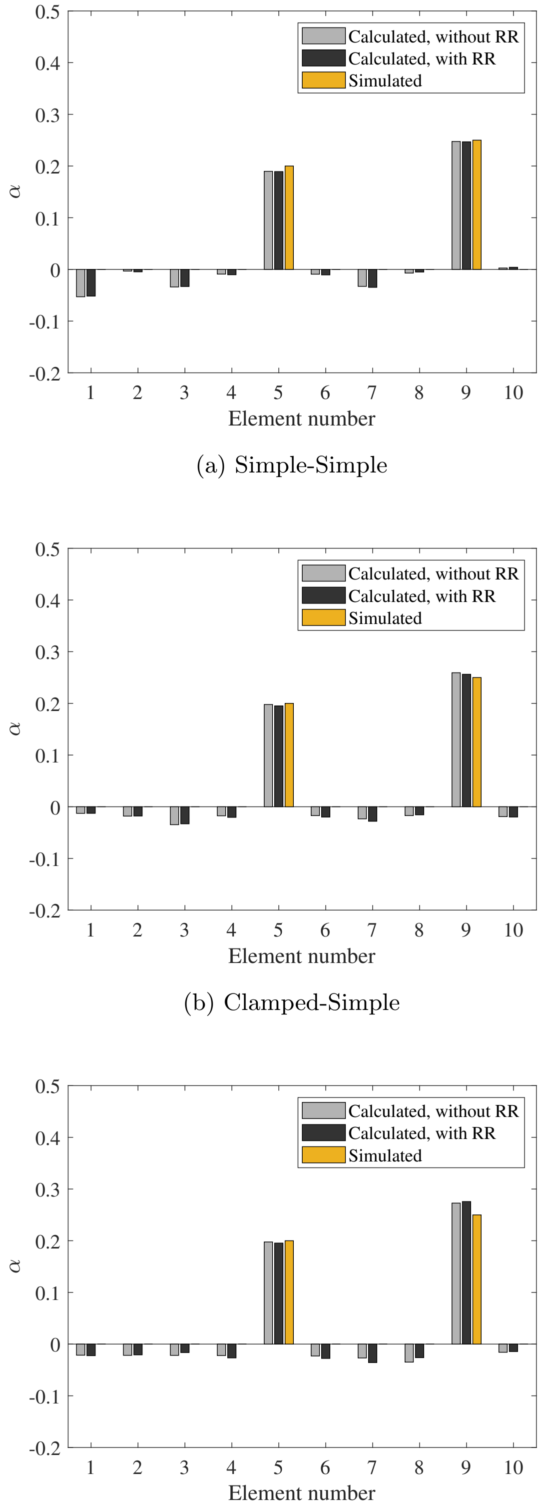

(a) Simple-Simple

(b) Clamped-Simple

(c) Clamped-Clamped

Figure 8: Calculated damage for the damaged beam scenario with different boundary conditions (actual damage indices are shown for comparison).

4.2. Effect of measurement noise on results

In order to simulate noisy measured data, 2% noise is added to all simulated data as outlined in [8],

$$\hat{\delta} = \delta + \frac{\kappa}{100} n_{\text{noise}}\, \sigma(\delta) \tag{29}$$

where $\hat{\delta}$ is the vector of noisy measured DOF data, and δ is the corresponding noise-free vector, which has standard deviation $\sigma(\delta)$. κ is the noise level in percent and n_{noise} is a vector with the same length as δ of random independent variables following a standard normal distribution.

Figures 9 and 10, show box-and-whisker plots of results obtained from 100 simulations with noise for the undamaged and damaged beam respectively. In these plots, the 'box' indicates the interquartile range and the median, while the 'whiskers' show extreme values, excluding outliers. Outliers, indicated (if they exist) by +, are defined as points outside approximately 2.7 standard deviations (99.3% coverage) for normally distributed data [51].

The results show that the statistics obtained for all cases with and without road roughness are very similar to each other. Moreover, as can be seen from these figures, the medians are very close to the exact values for both the undamaged and damaged cases, however in both cases the standard deviation of calculated damage indices is large for elements that coincide with the points of inflection in the fundamental vibration mode shape. These are the elements that will have maximum rotations, which may account for the higher uncertainty since the rotations were not assumed to be measured. On the other hand these elements are less likely to become damaged since they will tend to have close to zero curvature for more time. Importantly though, the distributions for the damaged and adjacent undamaged elements in Figure 10 do not overlap, so the detection of damage is significant.

It is also observed from the plots that, in most cases, the calculated results for damage indices are evenly distributed on both sides of the calculated medians, suggesting that the medians are almost the same as the mean values. For instance, for the damaged *CC* beam without road roughness the calculated median and mean values for α_5 are 0.2009 and 0.2005, respectively, a difference of 0.2%. The corresponding median and mean values of α_5 for the damaged *CC* beam with road roughness are calculated respectively 0.1945 and 0.1956 with slightly bigger difference of about 0.6%.

Figure 11 shows the the normal distribution curve fitted to the actual histograms for the damaged elements using the MATLAB function `histfit`.

It is seen that the averages obtained after a few simulations are close to the exact solution. This suggests that relatively precise results may be obtained by conducting the experiments a few times. Moreover, the fact that the proposed algorithm uses the integral of the vibration time

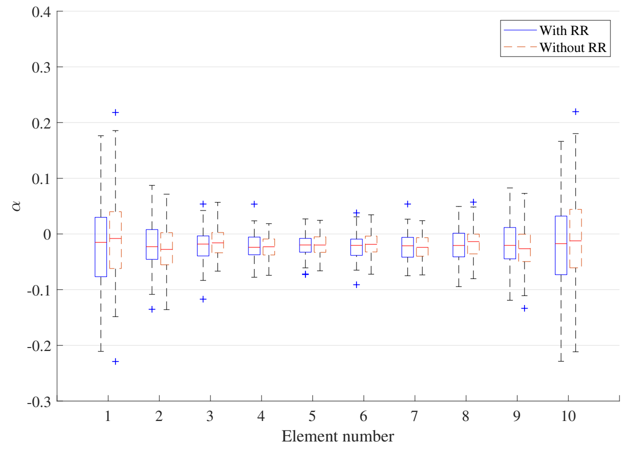

(a) Simple-Simple

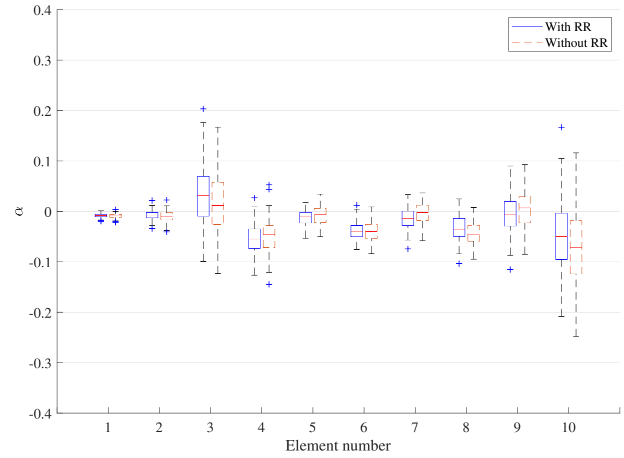

(b) Clamped-Simple

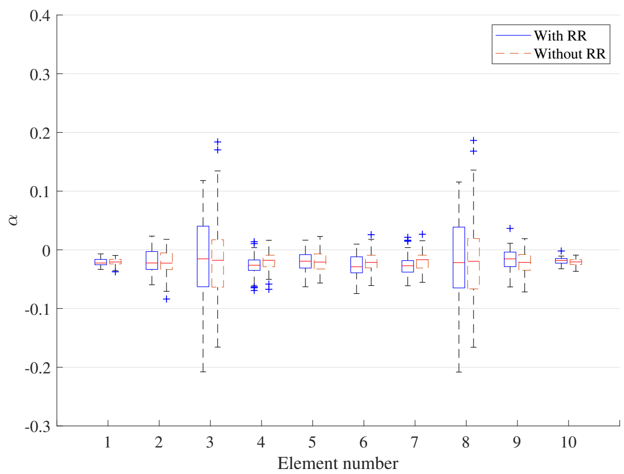

(c) Clamped-Clamped

Figure 9: Box plot for the calculated damage for the undamaged scenario of the beam with different boundary conditions using noisy measurements after 100 simulations.

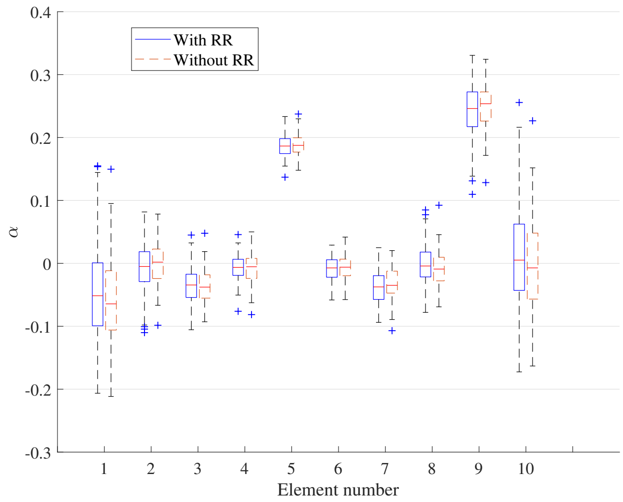

(a) Simple-Simple

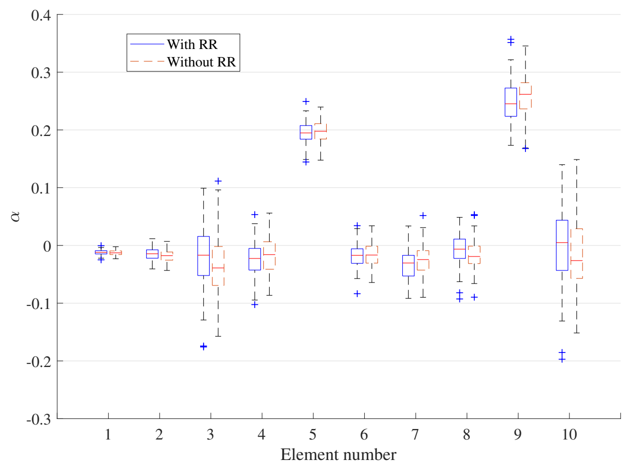

(b) Clamped-Simple

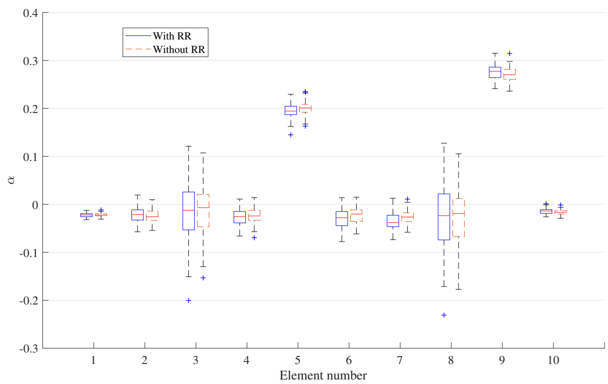

(c) Clamped-Clamped

Figure 10: Box plot for the calculated damage for the damaged scenario of the beam with different boundary conditions using noisy measurements after 100 simulations.

https://doi.org/10.1016/j.measurement.2020.108957

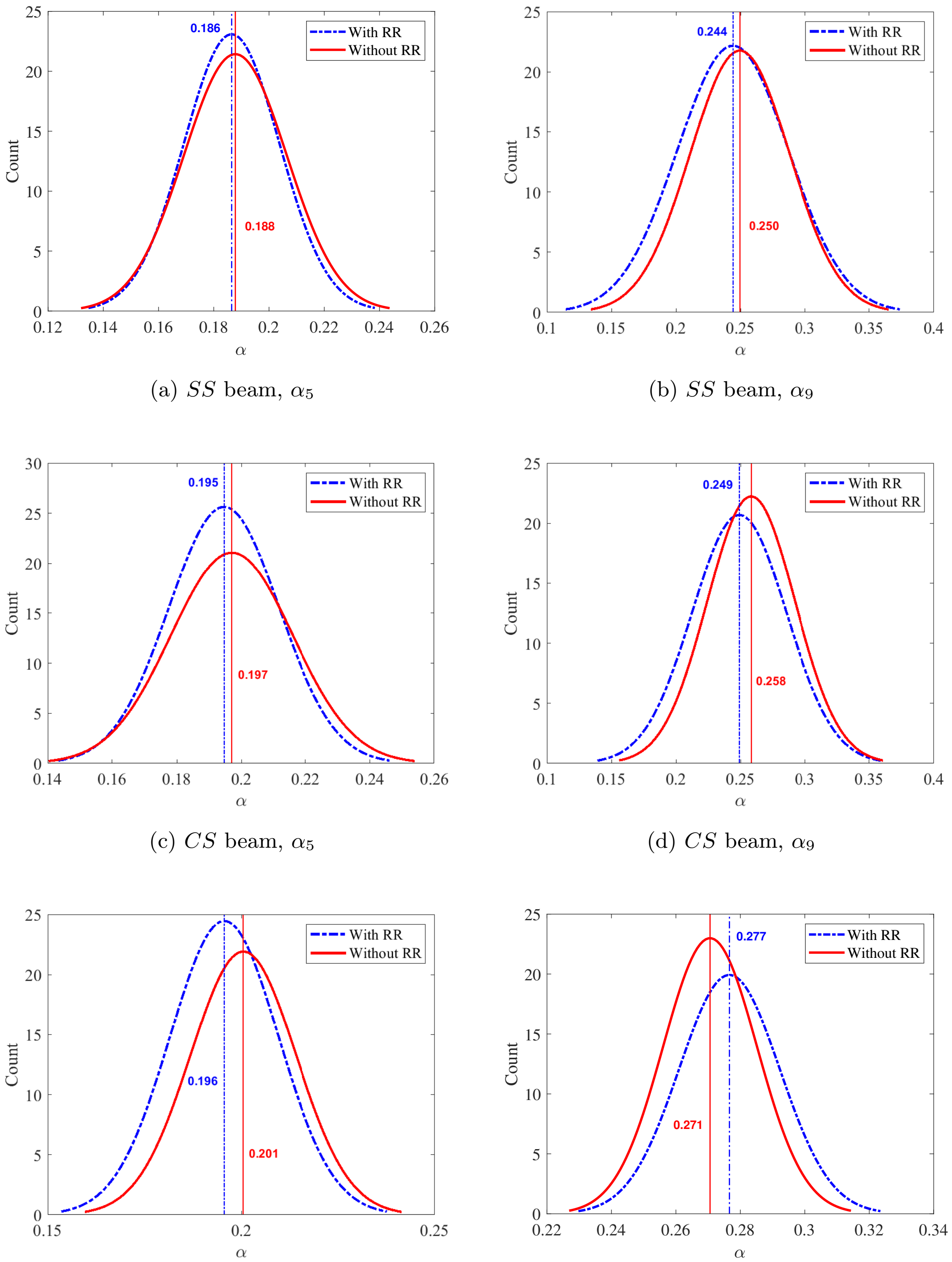

(a) SS beam, α_5

(b) SS beam, α_9

(c) CS beam, α_5

(d) CS beam, α_9

(e) CC beam, α_5

(f) CC beam, α_9

Figure 11: Fitted histogram to the obtained results after 100 times of simulation.

history of the beam can account for the reduction in the effect of the noise in calculated damage indices.

4.3. Further investigations of noise effects

In this part we consider the general damaged scenario when the road roughness effects are taken into account. Two different noise percentage are used for simulations, namely 2% and 5%. Figure 12 shows the obtained mean values of the damage indices. As it is apparent from the figure, the mean value of the calculated damage indices converges to a reasonable value fairly quickly when having 2% noise in measurements.

It is noted from the Figure 12a, that more experiments are required for the SS case than the other cases (CS and CC) to converge to a solution. As expected, more experiments are required with 5% noise in measurements to achieve the same convergence for the mean damage indices. As before, it can be seen in Figure 12b that a few more experiments are needed to achieve the average value of the calculated damage indices converged for the SS beam.

4.4. Variation of velocity of the moving mass

In this section, the capability of the proposed method is evaluated when the velocity of the mass varies along the beam. To that end, without loss of generality, it is assumed that the velocity of the mass is constant along each element while varying from one element to another, only for the sake of simplifying the simulation process. A general case is considered when the road roughness (RR) is present and all measurements are contaminated by 2% or 5% noise. Figure 13 shows the profile of the moving mass velocity, varying within a range 1.0–2.5 (m/s).

Note that Equation 25 was derived for the case of a constant moving mass velocity and therefore cannot be used in this case. As such, the more general case for $\{F\}$ given in Equation 23 must be evaluated, separated into vectors corresponding to slave and master DOFs, and substituted into Equation 11 to obtain $\{\bar{F}\}$, which is then substituted into Equation 9 to calculate the damage indices.

Accordingly, based on the results of Section 4.2 and 4.3, the mean values of the obtained damage indices from three experiments with a 2% and 5% measurement noise levels are presented in Figure 14 for the SS, CS, and CC beams.

The metric AI calculated for the SS, CS, and CC cases with 2% noise are 0.9626, 0.9624, and 0.9690 respectively, suggesting that results for the CC beam are most accurate, while results for the SS and CS beams are of almost equally accuracy. However, these results hardly differ from the constant velocity case (Table 4). If we further assume that the negative α values represent

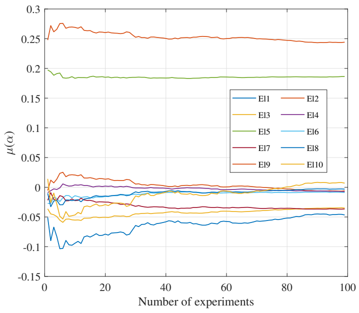

(a) Simple-Simple, 2% noise

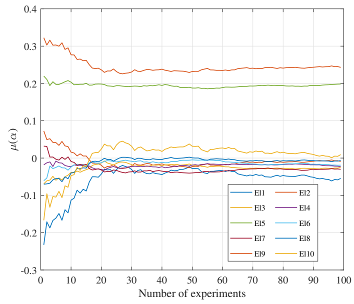

(b) Simple-Simple, 5% noise

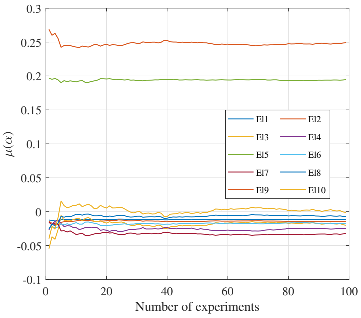

(c) Clamped-Simple, 2% noise

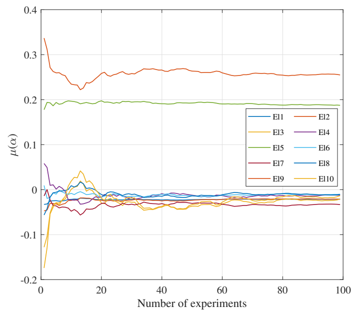

(d) Clamped-Simple, 5% noise

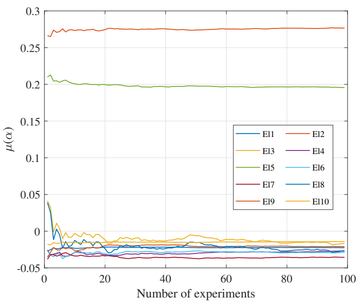

(e) Clamped-Clamped, 2% noise

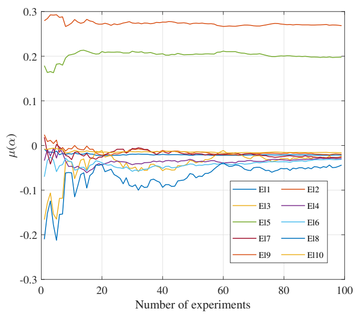

(f) Clamped-Clamped, 5% noise

Figure 12: Mean value of the damage indices per the number of simulations using 2% and 5% of noise in measurements.

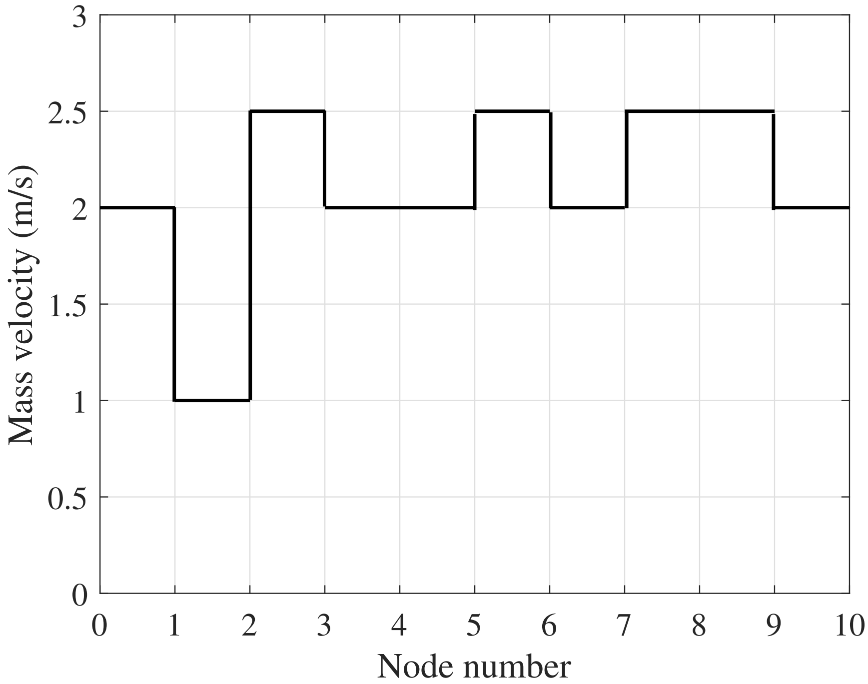

Figure 13: The mass is passing across the beam with varying velocity.

undamaged elements, as argued in Section, 4.1 the AI obtained for the CC beam in particular suggests very good accuracy.

The corresponding values for the case of 5% noise are 0.9560, 0.9552 and 0.9738 for SS, CS, and CC cases, respectively. Again better accuracy is obtained for the CC beam while the AI remains almost the same for SS and CS beams.

5. Conclusions and future work

In this paper a novel method is proposed to detect damage in beam type structures with different boundary conditions by using data from moving mass experiments and an equivalent static formulation of the dynamic vibration of the beam. The basic characteristic of the proposed method is that it uses a direct equation to obtain damage indices. Also the proposed method does not require any baseline information. We showed, analytically and numerically, that the proposed method yields good results in terms of damage detection in beam structure subjected to a moving mass considering road roughness effects and measurement noise.

Numerical examples of beams with different boundary conditions subjected to moving mass were studied in this paper. For this, scenarios of undamaged and damaged beams were investigated. It was shown that by introducing 2% and 5% noise to simulated data, the results are still within an acceptable range. It was also observed that the calculated damage indices for elements in the vicinity of nodes with maximum rotation (i.e. those near points of inflection

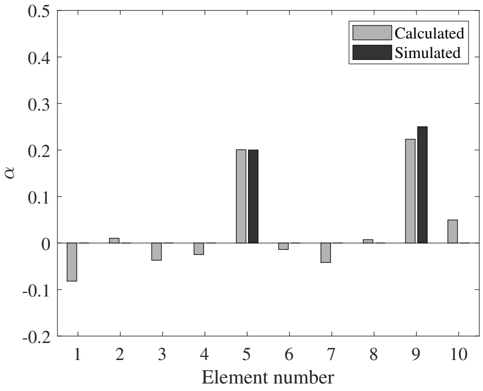

(a) Simple-Simple, 2% noise

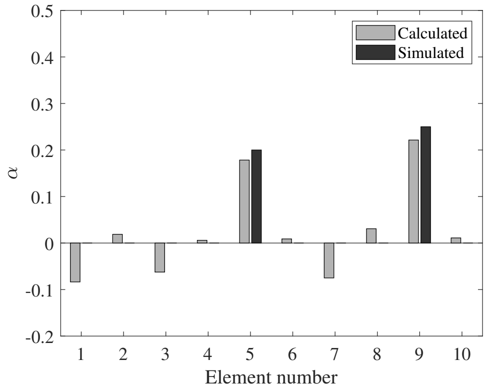

(b) Simple-Simple, 5% noise

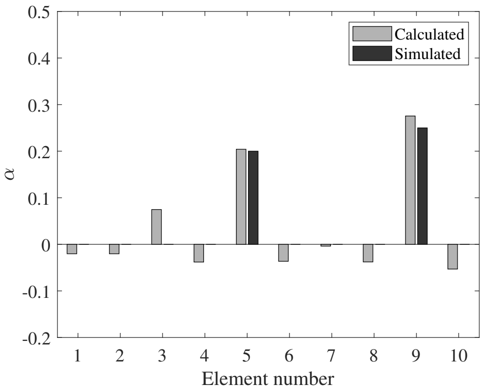

(c) Clamped-Simple, 2% noise

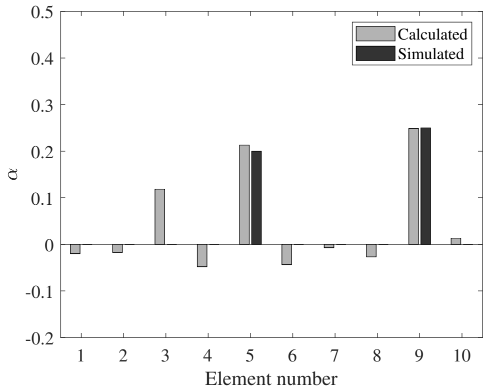

(d) Clamped-Simple, 5% noise

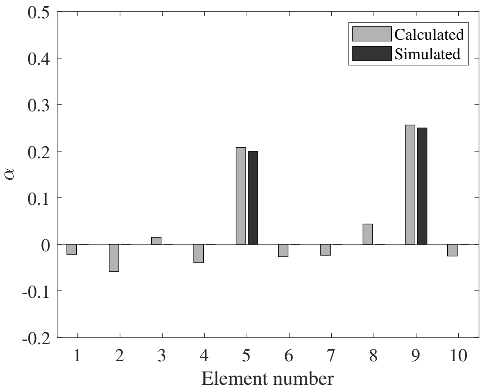

(e) Clamped-Clamped, 2% noise

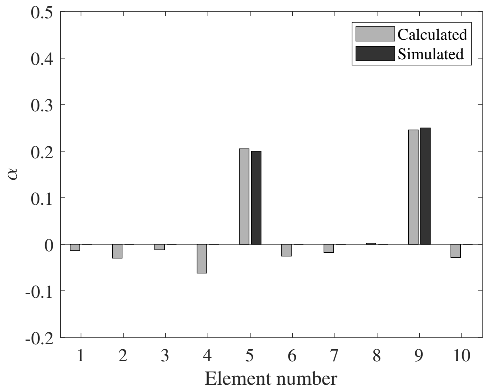

(f) Clamped-Clamped, 5% noise

Figure 14: Calculated damage for the damaged scenario applied to the SS, CS, and CC beams when using variable moving mass velocity with 2% and 5% noise in measurements after three times experiments.

in the fundamental vibration mode shape) are more prone to error. In all cases similar results are obtained for beams with and without road roughness effect. This proves that the proposed damage detection method is relatively insensitive to road profile effects. It has been also demonstrated that the proposed technique can be used with substantial variation of the moving mass velocity and the results are hardly affected.

The authors however, are aware that the further investigation of the applicability of the proposed method to real problems is a challenge and should be considered as a topic of future work.

References

[1] Y. An, E. Chatzi, S.-H. Sim, S. Laflamme, B. Blachowski, J. Ou, Recent progress and future trends on damage identification methods for bridge structures, Structural Control and Health Monitoring (2019) e2416.

[2] S. M. H. Pooya, A. Massumi, A novel and efficient method for damage detection in beam-like structures solely based on damaged structure data and using mode shape curvature estimation, Applied Mathematical Modelling 91 (2021) 670–694.

[3] G. Sha, M. Radzienski, R. Soman, M. Cao, W. Ostachowicz, W. Xu, Multiple damage detection in laminated composite beams by data fusion of teager energy operator-wavelet transform mode shapes, Composite Structures 235 (2020) 111798.

[4] R. Janeliukstis, S. Rucevskis, M. Wesolowski, A. Chate, Experimental structural damage localization in beam structure using spatial continuous wavelet transform and mode shape curvature methods, Measurement 102 (2017) 253–270.

[5] S. Stoykov, E. Manoach, Damage localization of beams based on measured forced responses, Mechanical Systems and Signal Processing 151 (2021) 107379.

[6] Y. Yang, Z. Wang, K. Shi, H. Xu, X. Mo, Y. Wu, Two-axle test vehicle for damage detection for railway tracks modeled as simply supported beams with elastic foundation, Engineering Structures 219 (2020) 110908.

[7] M. Jiang, W. Zhang, Q. Lu, A nonlinearity measure-based damage location method for beam-like structures, Measurement 146 (2019) 571–581.

[8] W.-Y. He, W.-X. Ren, S. Zhu, Damage detection of beam structures using quasi-static moving load induced displacement response, Engineering Structures 145 (2017) 70–82.

[9] G. James, T. Cao, M. Kaouk, D. Zimmerman, A coupled approach for structural damage detection with incomplete measurements, in: Topics in Modal Analysis, Vol. 7, Springer, 2014, pp. 141–153.

[10] S. Kourehli, Structural damage diagnosis using incomplete static responses and LS-SVM, Inverse Problems in Science and Engineering 25 (3) (2017) 418–433.

[11] T. Yin, Q.-H. Jiang, K.-V. Yuen, Vibration-based damage detection for structural connections using incomplete modal data by Bayesian approach and model reduction technique, Engineering Structures 132 (2017) 260–277.

[12] E. L. Eskew, S. Jang, Remaining stiffness estimation of buildings using incomplete measurements, Structural Control and Health Monitoring 24 (4) (2017).

[13] J. Yang, X. Liao, X. Yuan, P. Llull, D. J. Brady, G. Sapiro, L. Carin, Compressive sensing by learning a Gaussian mixture model from measurements, IEEE Transactions on Image Processing 24 (1) (2015) 106–119.

[14] Z. Zou, Y. Bao, H. Li, B. F. Spencer, J. Ou, Embedding compressive sensing-based data loss recovery algorithm into wireless smart sensors for structural health monitoring, IEEE Sensors Journal 15 (2) (2015) 797–808.

[15] J. G. Brida, L. F. Punzo, Symbolic time series analysis and dynamic regimes, Structural Change and Economic Dynamics 14 (2) (2003) 159–183.

[16] A. Khatkhate, A. Ray, E. Keller, S. Gupta, S. C. Chin, Symbolic time-series analysis for anomaly detection in mechanical systems, IEEE/ASME Transactions on Mechatronics 11 (4) (2006) 439–447.

[17] A. Cury, C. Cremona, Novelty detection based on symbolic data analysis applied to structural health monitoring, in: Proceedings of the Fifth International Conference on Bridge Maintenance, Safety and Management, IABMAS, Vol. 10, 2010, pp. 267–276.

[18] M. A. Fakih, S. Mustapha, M. Makki Alamdari, L. Ye, Symbolic dynamics time series analysis for assessment of barely visible indentation damage in composite sandwich structures based on guided waves, Journal of Composite Materials 51 (29) (2017) 4129–4143.

[19] M. Makki Alamdari, B. Samali, J. Li, Y. Lu, S. Mustapha, Structural condition assessment using entropy-based time series analysis, Journal of Intelligent Material Systems and Structures 28 (14) (2017) 1941–1956.

[20] M. Mousavi, D. Holloway, J. Olivier, A. H. Alavi, A. H. Gandomi, A shannon entropy approach for structural damage identification based on self-powered sensor data, Engineering Structures 200 (2019) 109619.

[21] X. Zhu, S. Law, Wavelet-based crack identification of bridge beam from operational deflection time history, International Journal of Solids and Structures 43 (7-8) (2006) 2299–2317.

[22] V. Pakrashi, A. O'Connor, B. Basu, A bridge-vehicle interaction based experimental investigation of damage evolution, Structural Health Monitoring 9 (4) (2010) 285–296.

[23] J. N. Yang, Y. Lei, S. Lin, N. Huang, Hilbert-Huang based approach for structural damage detection, Journal of Engineering Mechanics 130 (1) (2004) 85–95.

[24] N. Cheraghi, F. Taheri, A damage index for structural health monitoring based on the empirical mode decomposition, Journal of Mechanics of Materials and Structures 2 (1) (2007) 43–61.

[25] J. Meredith, A. González, D. Hester, Empirical mode decomposition of the acceleration response of a prismatic beam subject to a moving load to identify multiple damage locations, Shock and Vibration 19 (5) (2012) 845–856.

[26] M. Mousavi, D. Holloway, J. Olivier, A. H. Gandomi, Beam damage detection using synchronisation of peaks in instantaneous frequency and amplitude of vibration data, Measurement 168 (2021) 108297.

[27] H. Mahgoun, F. Chaari, A. Felkaoui, Detection of gear faults in variable rotating speed using variational mode decomposition (vmd), Mechanics & Industry 17 (2) (2016) 207.

[28] W.-Y. He, S. Zhu, Moving load-induced response of damaged beam and its application in damage localization, Journal of Vibration and Control 22 (16) (2016) 3601–3617.

[29] M. Link, M. Weiland, Damage identification by multi-model updating in the modal and in the time domain, Mechanical Systems and Signal Processing 23 (6) (2009) 1734–1746.

[30] W. Zhang, J. Li, H. Hao, H. Ma, Damage detection in bridge structures under moving loads with phase trajectory change of multi-type vibration measurements, Mechanical Systems and Signal Processing 87 (2017) 410–425.

[31] B. Zhang, Y. Qian, Y. Wu, Y. Yang, An effective means for damage detection of bridges using the contact-point response of a moving test vehicle, Journal of Sound and Vibration 419 (2018) 158–172.

[32] W.-Y. He, J. He, W.-X. Ren, Damage localization of beam structures using mode shape extracted from moving vehicle response, Measurement 121 (2018) 276–285.

[33] K. V. Nguyen, Comparison studies of open and breathing crack detections of a beam-like bridge subjected to a moving vehicle, Engineering Structures 51 (2013) 306–314.

[34] N. Roveri, A. Carcaterra, Damage detection in structures under traveling loads by Hilbert-Huang transform, Mechanical Systems and Signal Processing 28 (2012) 128–144.

[35] E. J. OBrien, A. Malekjafarian, A. González, Application of empirical mode decomposition to drive-by bridge damage detection, European Journal of Mechanics-A/Solids 61 (2017) 151–163.

[36] W.-Y. He, W.-X. Ren, S. Zhu, Baseline-free damage localization method for statically determinate beam structures using dual-type response induced by quasi-static moving load, Journal of Sound and Vibration 400 (2017) 58–70.

[37] M. Mousavi, D. Holloway, J. Olivier, A new signal reconstruction for damage detection on a simply supported beam subjected to a moving mass, Journal of Civil Structural Health Monitoring 10 (4) (2020) 709–728.

[38] K. Jarczewska, P. Koszela, P. Śniady, A. Korzec, Identification of the structure parameters using short-time non-stationary stochastic excitation, Journal of Sound and Vibration 330 (14) (2011) 3352–3367.

[39] M. Mousavi, A. H. Gandomi, An input–output damage detection method using static equivalent formulation of dynamic vibration, Archives of Civil and Mechanical Engineering 18 (2) (2018) 508–514.

[40] J. Li, S. Law, Damage identification of a target substructure with moving load excitation, Mechanical Systems and Signal Processing 30 (2012) 78–90.

[41] D.-M. Chen, Y. Xu, W. Zhu, Non-model-based multiple damage identification of beams by a continuously scanning laser doppler vibrometer system, Measurement 115 (2018) 185–196.

[42] R. U. A. Uzzal, R. B. Bhat, W. Ahmed, Dynamic response of a beam subjected to moving load and moving mass supported by pasternak foundation, Shock and Vibration 19 (2) (2012) 205–220.

[43] Y. Yang, C. Lin, Vehicle bridge interaction dynamics and potential applications, Journal of Sound and Vibration 284 (1–2) (2005) 205–226. doi:10.1016/j.jsv.2004.06.032.

[44] S. Oller, A. H. Barbat, Moment–curvature damage model for bridges subjected to seismic loads, Computer Methods in Applied Mechanics and Engineering 195 (33-36) (2006) 4490–4511.

[45] M. Kurata, J.-H. Kim, J. P. Lynch, K. H. Law, L. W. Salvino, A probabilistic model updating algorithm for fatigue damage detection in aluminum hull structures, in: ASME 2010 Conference on Smart Materials, Adaptive Structures and Intelligent Systems, American Society of Mechanical Engineers, 2010, pp. 741–750.

[46] A. Ben-Israel, T. N. Greville, Generalized inverses: theory and applications, Vol. 15, Springer Science & Business Media, 2003.

[47] G. Strang, 18.06 sc linear algebra, fall 2011, left and right inverses; pseudoinverse, Massachusetts Institute of Technology: MIT OpenCourseWare (2011).

[48] S. S. Rao, The finite element method in engineering, Butterworth-heinemann, 2017.

[49] M. Agostinacchio, D. Ciampa, S. Olita, The vibrations induced by surface irregularities in road pavements—a Matlab® approach, European Transport Research Review 6 (3) (2014) 267–275.

[50] M. Mousavi, A. H. Gandomi, A hybrid damage detection method using dynamic-reduction transformation matrix and modal force error, Engineering Structures 111 (2016) 425–434.

[51] J. W. Tukey, Exploratory data analysis, Vol. 2, Reading, Mass., 1977.